AIAA 98-2941

LAMINAR-TO-TURBULENT TRANSITION PREDICTION AROUND THE MUSES-C REENTRY CAPSULE

K. KOMURASAKI
Nagoya University
Nagoya, Japan
and
G.V. CANDLER
University of Minnesota
Minneapolis, MN

7th AIAA/ASME Joint Thermophysics and Heat Transfer Conference
June 15-18, 1998 / Albuquerque, NM

For permission to copy or republish, contact the American Institute of Aeronautics and Astronautics
1801 Alexander Bell Drive, Suite 500, Reston, VA 20191

LAMINAR-TO-TURBULENT TRANSITION PREDICTION AROUND THE MUSES-C REENTRY CAPSULE

Kimiya KOMURASAKI
Department of Aerospace Engineering, Nagoya University
Chikusa, Nagoya 464-01, Japan
and
Graham V. CANDLER
Department Aerospace Engineering and Mechanics, University of Minnesota
110 Union St. SE, Minneapolis, MN 55455

Abstract

Laminar-to-turbulent transition over an ablator heat-shield of the MUSES-C reentry capsule has been analytically predicted. A two-equation turbulence model (k-ε model) was coupled with Reynolds averaged Navier-Stokes equations to reproduce the boundary flow transition. The low-Reynolds-number effect on the solid wall boundary was taken into account by modifying the Chien's correction. The results show that the turbulence induced by turbulent-gas-injection from the ablator surface was multiplied in a boundary layer, and the flow transited to turbulence. The predicted transition point Reynolds number was 3×10^4 at the surface mass injection rate of 100 g/sm^2.

Nomenclature

C_p : specific heat at constant pressure
d : Park's mixing length on the turbulent wall
E : total energy per unit mass
F, G : flux vectors in x and r directions, respectively
k : turbulence kinetic energy per unit mass
K : Von Karman constant, 0.41
p : static pressure
Pr : Prandtl number
q : heat flux
R : nose radius, 0.2 m
Re : Reynolds number, $\rho_\infty V_\infty R/\mu_\infty$
Re_{tr} : transition point Re, $\rho_\infty V_\infty s_{tr}/\mu_\infty$
s : distance from stagnation point along the body contour
t : time
T : temperature
T_i : turbulent intensity, $T_i = \sqrt{2k/3v_w^2}$
u, v : mean velocity components
u', v' : fluctuating velocity components
u_τ : friction velocity, $u_\tau = \sqrt{\tau_W/\rho}$
U : vector of conservative variables
W : source vector
x, r, θ : cylindrical polar coordinates
y : wall normal distance
y^+ : wall variable, $y^+ = y(u_\tau/\nu)$
ε : turbulence dissipation rate
γ : specific heat ratio
κ : thermal conductivity
μ_M : molecular viscosity
μ_T : eddy viscosity
ν : kinematic molecular viscosity
ρ : density
τ : shear stress

Subscript
I : inviscid
SP : stagnation point
T : turbulent
tr : transition
V : viscous
W : wall condition
∞ : free-stream condition

Introduction

The Institute of Space and Astronautical Sciences of Japan has proposed a space program MUSES-C, in which a spacecraft will rendezvous with an asteroid and bring samples of the asteroid material back to Earth by a reentry capsule.[1] The spacecraft is scheduled to be launched in 2002 to rendezvous with an asteroid Nereus, and return in 2006. The atmospheric reentry speed will exceed 12 km/s, corresponding reentry Mach number is 42.

The laminar shock layer analyses conducted on this mission indicate that the maximum convective heat transfer rate on the capsule surface would be approximately 10 MW/m^2 and the radiative rate about 2 MW/m^2. In order to survive such an extremely high heating rate, the reentry capsule is shielded with a carbon-phenolic ablator. From a material test using an arc-heater, the recession rate of the ablator has been

Copyright © 1998 The American Institute of Aeronautics and Astronautics Inc. All right reserved.

estimated as 100 g/sm^2 at the heating rate of 10 MW/m^2. [2] This surface-mass-flux corresponds to several % of free-stream mass-flux. Such a large amount of surface-mass-injection might induce turbulence even near the stagnation point of the capsule,[3-5] resulting in a higher heating rate than predicted by laminar flow analyses.

Several experimental studies on laminar-to-turbulent transitions over a body with surface-mass-injection have been done in the United States so far, and those results have shown the transition.[6,7]

Generally speaking, boundary flow transitions are hard to occur at the Re as low as the order of 10^4, at which heating rate would be maximum during the MUSES-C reentry. However, Kaattari's experiment predicted the transition $Re = 3 \times 10^4$. It implies that transition might occur in the MUSES-C mission. Such a low Re transition or "early" transition is thought to be caused by inhomogeneous and unsteady gas injection on the ablator surface. [3]

The objective of this study is to analytically predict the transition Reynolds number and the maximum heating rate over the ablator of MUSES-C reentry capsule.

Numerical model

Reynolds averaged Navier-Stokes equation

Reynolds averaged Navier-Stokes equations coupled with the standard k-ε turbulent model[8] over an axisymmetric blunt body are expressed as

$$\frac{\partial U}{\partial t} + \frac{\partial (F_I - F_V)}{\partial x} + \frac{1}{r}\frac{\partial r(G_I - G_V)}{\partial r} = W \qquad (1)$$

where

$$U = \begin{bmatrix} \rho \\ \rho u \\ \rho v \\ E \\ \rho k \\ \rho \varepsilon \end{bmatrix}, \quad F_I = \begin{bmatrix} \rho u \\ \rho u u + p \\ \rho v u \\ (E+p)u \\ \rho k u \\ \rho \varepsilon u \end{bmatrix},$$

$$F_V = \begin{bmatrix} 0 \\ \tau_{xx} + \tau_{xx}^T - 2/3\rho k \\ \tau_{xr} + \tau_{xr}^T \\ (\tau_{xx}+\tau_{xx}^T-2/3\rho k)u + (\tau_{xr}+\tau_{xr}^T)v + \kappa \partial_x T \\ (\mu_M + \mu_T)\partial_x k \\ (\mu_M + \mu_T/1.3)\partial_x \varepsilon \end{bmatrix},$$

$$W = \begin{bmatrix} 0 \\ 0 \\ (p - \tau_{\theta\theta})/r \\ 0 \\ (\tau^R \nabla)u - \rho\varepsilon \\ (\varepsilon/k)(1.44(\tau^R \nabla)u - 1.92\rho\varepsilon) \end{bmatrix},$$

$$E = \rho/(\gamma - 1) + .5\rho(u^2 + v^2) + \rho k \qquad (2)$$

Transport coefficients

In the first-order turbulent closure model, the Reynolds shear stress τ^R is expressed through the eddy viscosity, following Boussinesq's assumption:

$$\tau_{ij}^R = \tau_{ij}^T - (2/3)\rho k \delta_{ij} \qquad (3)$$

$$\tau_{ij}^T = \mu_T(\partial_i u_j + \partial_j u_i - (2/3)\nabla \cdot u \delta_{ij}) = (\mu_T/\mu_M)\tau_{ij} \qquad (4)$$

In the standard k-ε model, the eddy viscosity is expressed as:

$$\mu_T = 0.09\rho k^2/\varepsilon \qquad (5)$$

Thermal conductivity coefficient can be defined through the Prandtl numbers. Assuming the laminar and turbulent Prandtl numbers for air flow to be constant as 0.72 and 0.9, respectively, total thermal conductivity is expressed as:

$$\kappa = C_p(\mu_M/0.72 + \mu_T/0.9) \qquad (6)$$

In this study, neither chemical reactions nor real gas effects are taken into account, because we focus on transition mechanism through mechanical properties of the flow. Because of this, calculated post-shock temperature goes up to 80,000 K, which is several times higher than actual post-shock temperature. The molecular viscosity coefficient is obtained using an approximation for non-reacting air with a chemical composition frozen at standard conditions.[9]

$$\mu_M = 1.462\times10^{-6} T^{1/2}/(1+112/T) \ \text{kg/ms} \qquad (7)$$

Low-Reynolds-number effect

In order to accurately predict the boundary flow transition, limiting behavior of the fluctuating velocities approaching a solid boundary has to be considered. This effect has been expressed in following corrections as: 1) "non-isotropic dissipation" of turbulent energy, and 2) a "damping" effect on eddy viscosity, by Jones and Launder,[10] Launder and Sharma,[11] Chien, [12] etc.

If the body surface is smooth and non-ablative, the fluctuating velocity satisfies the no-slip boundary condition and also satisfies conservation of mass. Therefore, from expanding the fluctuating velocity in Taylor series near a solid boundary, the tangential and

normal components u' and v' must behave as

$$u' = A(s,t)y + O(y^2), \quad v' = B(s,t)y^2 + O(y^3) \quad (8)$$

respectively, as $y \rightarrow 0$.

The behavior of k and ε is deduced from these asymptotic variations of fluctuation velocities as:

$$k = \overline{u'^2 + v'^2} = \overline{A^2}\, y^2 + O(y^3),$$
$$\varepsilon = \nu\overline{(u'^2_{,y} + v'^2_{,y})} = \overline{A^2} + O(y) \quad (9)$$

k decreases rapidly as $y \rightarrow 0$, while ε remains finite at $y = 0$. This is the "non-isotropic dissipation" of turbulent energy. To achieve this asymptotic consistency, the "wall" dissipation, ε_0 is added to the turbulent energy equation in most of the low-Reynolds-number corrections. In Chien's correction, ε_0 is expressed as:

$$\varepsilon_0 = 2\nu k / y^2 \quad (10)$$

To include the "damping" effect on eddy viscosity, Eq. (5) is often modified using a damping function, f_μ as:

$$\mu_T = 0.09 f_\mu \rho k^2 / \varepsilon \quad (11)$$

In Chien's correction, f_μ depends on a wall variable, y^+.

$$f_\mu = 1 - \exp(-0.0115 y^+) \quad (12)$$

However, in the case of a charring ablator such as a carbon-phenolic one, there can exist finite velocity fluctuations even at $y = 0$ as schematically shown in Fig. 1, because the ablation gas is ejecting at subsonic speed through porous char remnant and allows disturbances to propagate from the boundary flow into the ablator. Assuming the limiting case when the surface fluctuation velocities perfectly couple with the ones of the boundary flow, the "non-isotropic dissipation", ε_0 is neglected in this study.

As for the viscosity "damping" effect, eddy viscosity should go to zero as $y^+ \rightarrow 0$ as indicated in Eqs. (11) and (12). This effect preserves boundary flows from transition until $Re = 10^5 \sim 10^6$. Nevertheless, when the ablation gas is turbulent, eddy does not vanish on the surface. In order to take account of the eddy scale on the ablator surface, we define a new wall variable using a non-zero wall variable on the wall, y_w^+ as:

$$y^+ = y(u_\tau/\nu) + y_w^+ \quad (13)$$

In this study, two cases are discussed; 1) the eddy scale is roughly larger than boundary layer thickness so that the damping effect is negligible:

$$y_w^+ = \infty \quad (14)$$

and 2) the eddy scale is given by the Park's wall mixing length model[3] as:

$$y_w^+ = (d/K)(u_\tau/\nu), \quad (15)$$

$$d = \tau_e v_w \quad (16)$$

Here, d is the Park's wall mixing length and v_w is the mean injection velocity. A time constant, τ_e is an average time interval of fluctuation of injected flow. A reasonable value of the time constant can be taken to be $\tau_e = 2 \times 10^{-4}$ s for carbon-carbon composite.

Although two more damping functions are usually added to the dissipation equation in the low-Reynolds-number corrections, they are neglected here because these effects are quite small for the turbulent-surface condition.

Numerical scheme

FVS (Flux Vector Splitting) method is often used for calculating hypersonic blunt-body flow-fields, because of its robustness and suitability for use in implicit schemes,[13] while it comes at a price of reduced accuracy due to numerical dissipation. The numerical dissipation is especially unfavorable to the turbulence calculation because it is essentially the calculation of turbulence-dissipation processes. On the other hand, FDS (Flux Difference Splitting) method is very accurate, though operation count and complexity are increased for complete linearization of flux formulas for implicit schemes.

Thereby, the AUSM (Advection Upstream Splitting Method) [14] is employed in this study. This scheme combines the efficiency of FVS and the accuracy of FDS, and enables us to efficiently capture the hypersonic shock and to accurately evaluate boundary layer flows. The Gauss-Seidel line relaxation method is adopted to implicitly solve the nonlinear equations.

Figure 2 is a plot of a 120 × 30 grid used in this study. The master equations were discretized with a third-order upwind scheme using the MUSCL type interpolation. A grid convergence was obtained for heat flux distribution and for transition position.

Boundary conditions

Free-stream

The free-stream Reynolds number is a key parameter for the amplification or suppression of eddy viscosity in the boundary layer. Reentry conditions at the flight altitude of 60 km and 76 km were tested corresponding to free-stream Re of 45000 and 6500, respectively. The free-stream conditions are listed in Table 1.

Table 1 Free-stream conditions.

76 km altitude	density	3.5×10^{-5} kg/m^3
	temperature	195 K
	Mach number	42
	Reynolds number	6500
60 km altitude	density	30.5×10^{-5} kg/m^3
	temperature	256 K
	Mach number	38
	Reynolds number	45000

(In the MUSES-C mission, the heating rate is predicted to have a peak at approximately 60 km of altitude.) The free-stream is assumed turbulence free.

Ablator surface

The surface temperature is assumed identical to 4000 K and the local injection rates are assumed in proportion to the local heating rates as:

$$\rho_W v_W = A\dot{q} \qquad (17)$$

The injection-rate can be tuned by changing the coefficient A.

The ablation gas is injected perpendicular to the surface with a given turbulent kinetic energy. The turbulent intensity on the surface is specified to 0.03 $\sim$0.3.

Since the dissipation boundary condition, ε_W doesn't give any distinguishable effect on the results, it was given so that $(0.09\rho k/\varepsilon^2)_W = (\mu_M)_W$.

Results

Case with $y_W^+ = \infty$

The calculated heating rate distributions over the capsule surface are shown in Fig. 3. In the case Re = 45000, the stagnation-point heating is decreased with an increase in surface injection rate due to the heat-blockage effect. Every plot shows an increase in heating rate in the downstream region due to the laminar-to-turbulent transition, except for the no-injection case. At the injection rate of 80 g/sm^2, heating rate has a peak at s =12 cm, and the maximum rate was approximately 25 % higher than the stagnation-point one.

In the case Re = 6500, the flow stayed laminar for any injection rate.

Figure 4 shows the profiles of mean velocity and turbulence kinetic energy in the case Re = 45000. The plots are enlarged in the surface normal direction by a factor of five. Turbulence kinetic energy is amplified in the stream-wise direction in the middle of boundary layer.

Figure 5 shows the distributions of the eddy viscosity and molecular viscosity. These plots are also enlarged in the surface normal direction. The eddy viscosity surpassed the molecular viscosity in the downstream region.

The peak eddy viscosity along the wall normal lines is plotted in the stream-wise direction in Fig. 6. It was normalized by the local molecular viscosity. The nonlinear amplification of the eddy viscosity indicates the transition. The transition point shifts upstream with an increase in the surface injection rate.

Case with $y_W^+ = (d/K)(u_\tau/\nu)$

Figure 7 shows the distributions of the heating rate and the peak eddy viscosity along the surface at the injection rate of 80g/sm^2. Comparing with Figs. 3 and 6, transition delayed due to the viscosity damping effect. The flow stayed laminar at the injection rate less than 80 g/sm^2.

Figure 8 shows the heating rate distributions for various injection rates. Transition occurs earlier with larger injection rates.

The distance from the stagnation point to the transition point is plotted for various surface turbulent intensity in Fig. 9. It shows a weak dependence on the surface turbulent intensity condition. This is due to the fact that the kinetic energy of the injection gas is much smaller than that of main flows, and the turbulent energy in the vicinity of surface is determined through the diffusion, $(\mu_T+\mu_M)\nabla k$ from the region where the flow is turbulent.

Owing to the same reason, the calculation is insensitive to the dissipation condition on the surface, ε_W as mentioned above.

If $T_i = 0$ on the surface, the flow stays laminar at any injection rate because there is no seed of turbulence.

Figure 10 shows a streamline of the gas injected near the stagnation point. The seed of turbulence given near the stagnation point is carried along the streamline and is gradually amplified by the work of the main flow against the Reynolds stress. The streamline is separated from the surface and swelled into the middle of boundary layer by successive gas injection in the downstream region of the surface. With the small injection rate, the streamline stays in the region where the viscosity damping is strong, while with the large injection rate, the streamline is pushed into the region where Re is relatively high and damping effect is weak, resulting in the transition.

Injection rate and transition point Re

Figure 11 shows a comparison between the Kaattari's transition experiment and the present prediction. The injection rate normalized by free-stream mass-flux is on the abscissa and the transition point Re is on the ordinate.

In the case with $y_W^+ = \infty$, calculated results show earlier transition than the experimental prediction. Transition occurs even at the quite small injection rate. On the other hand, in the case with $y_W^+ = (d/K)(u_\tau/\nu)$, transition doesn't occur at the injection rate less than 80g/sm^2. The calculated transition envelope is well agree with the experimental result.

Discussions

The mechanism for the early transition induced by surface mass injection would consist in following two points.

1) The reduction of viscosity damping due to the surface turbulent condition.

2) The swelling of stream-lines of the ablation gas by successive gas injection in the downstream region of the surface.

Both of them assist the amplification of eddy viscosity in boundary flows. These effects strongly depend on the ablation rate on the surface. That is consistent with Kaattari's experiment.

Since the predicted transition point *Re* shows good agreement with the experimental results, it can be concluded that this numerical model well represents the early transition mechanism due to surface mass injection

References

1) Park, C. and Abe, T. : Research on the Heatshield for MUSES-C Earth Reentry, 7th Joint Thermophysics and Heat Transfer Conference, AIAA Paper 98-2852, Albuquerque NW, 1998.

2) Ishii, N., Inatani, Y., Hiraki, K. and Yamada, T. : Thermal Protection system of Muses-C Reentry Capsule, 21st International Symposium on Space Technology and Science, Paper 98-d-04, Omiya, Japan, 1998.

3) Park, C. : Injection-Induced Turbulence in Stagnation-Point Boundary Layer, *AIAA Journal* Vol. 22, 1984, pp. 219-225.

4) Park, C. and Balakrishnan, A. : Ablation of Galileo Probe Heat-Shield Models in a Ballistic Range, *AIAA Journal*, Vol. 23, No. 2, 1985, pp. 301-308.

5) Laurien E. : Numerical Investigation of Laminar-Turbulent Transition on Re-Entry Capsules, *Journal of Spacecraft and Rockets*, Vol. 33, No. 3, 1996, pp. 313-318.

6) Demetriades, A., Laderman, A. J. and Von Seggern, L. : Effect of Mass Addition on the Boundary Layer of a Hemisphere at Mach 6, *Journal of Spacecraft and Rockets*, Vol. 13, No. 8, 1976, pp. 508-509.

7) Kaattari, G. E. : Effects of Mass Addition on Blunt-Body Boundary-Layer Transition and Heat Transfer, NASA Technical Paper 1139, 1979.

8) Launder, B. E. and Spalding, B. : Mathematical Models of Turbulence, New York Academic Press, 1972.

9) Hansen, C. F. : Approximation for the Thermodynamic and Transport Properties of High Temperature Air, NASA TR-R-50, 1959.

10) Jones, W. P. and Launder, B. E. : The Prediction of Laminalization with a two-equation Model of Turbulence, *International Journal of Heat Mass Transfer*, Vol. 15, 1972, pp. 301-314.

11) Launder, B. E. and Sharma, B. I. : Application of the Energy Dissipation Model of Turbulence to the Calculation of Flow Near a Spinning Disc, *Letters in Heat and Mass Transfer*, Vol. 1, No. 2, 1974, pp. 131-138.

12) Chien, K-Y. : Predictions of Channel and Boundary Layer Flows with a Low-Reynolds Number Turbulence Model, *AIAA Journal*, Vol. 20, No. 1, 1982, pp. 33-38.

13) Candler, G. V. and MacCormack, R. W. : The Computation Hypersonic Ionized Flows in Chemical and Thermal Nonequilibrium, *Journal of Thermophysics and Heat Transfer*, Vol. 5, No. 3, 1991, pp. 266-273.

14) Liou, M. S. and Steffen, C. J. : A New Flux Splitting Scheme, *Journal of Computational Physics*, Vol. 107, 1993 , pp. 23-39.

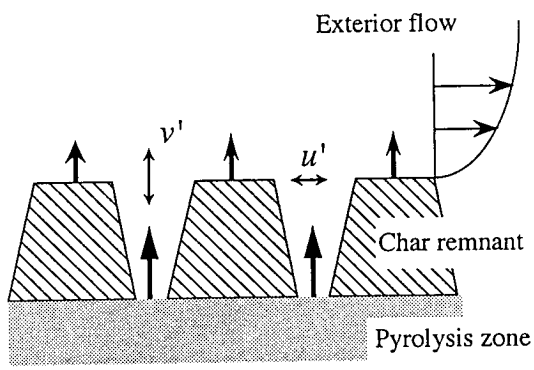

Fig. 1 Schematic of velocity fluctuations on a charring ablator.

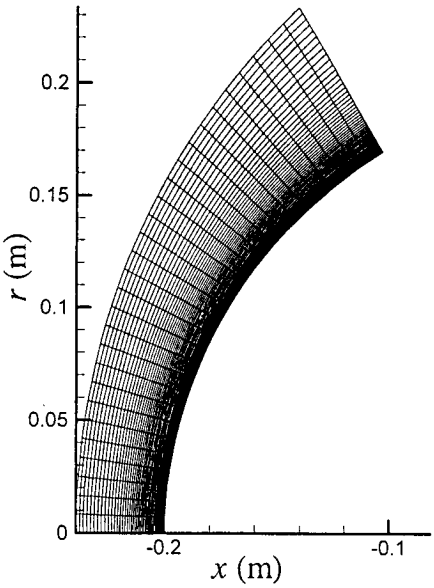

Fig. 2 Plot of a 120 × 30 grid.

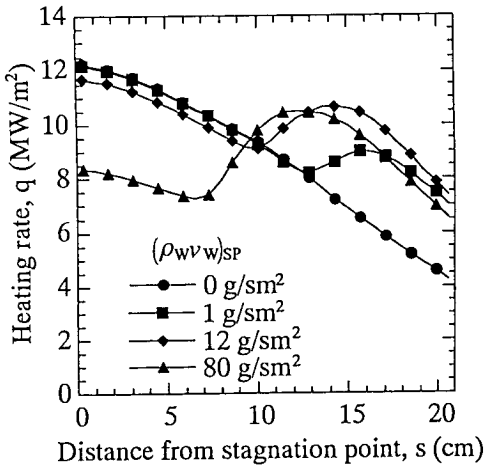

(a) Re = 45000

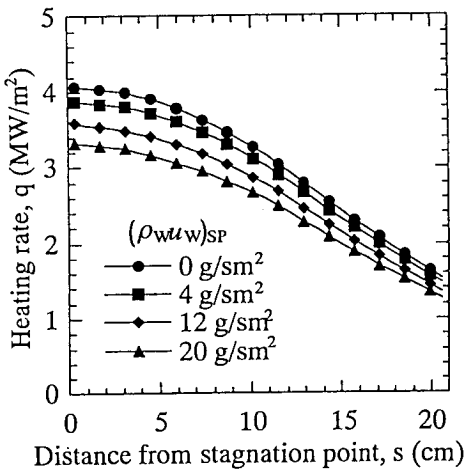

(b) Re = 6500

Fig. 3 Heating rate distributions on an ablator surface. $y_W^+ = \infty$, $T_i = 0.1$.

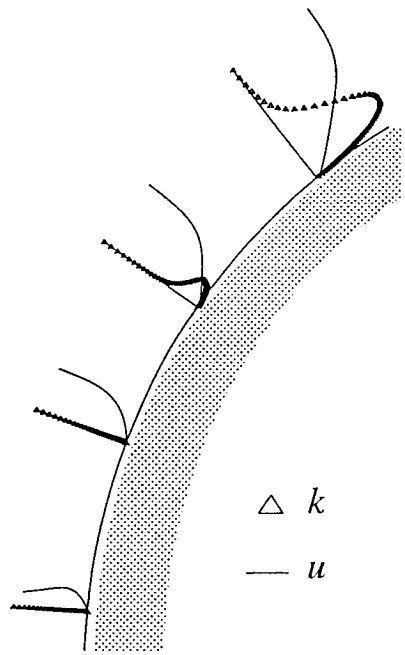

Fig. 4 Profiles of mean velocity and turbulent kinetic energy. Re =45000, $y_W^+ = \infty$, T_i =0.1, $(\rho_W \nu_W)_{SP}$ =80 g/sm². Enlarged in the wall normal direction by a factor of five.

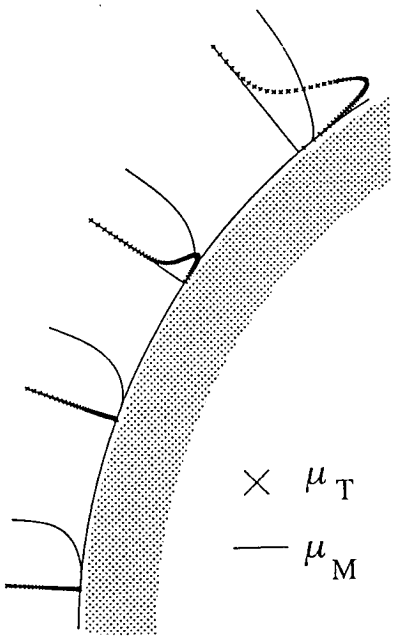

Fig. 5 Profiles of eddy viscosity and molecular viscosity. Re = 45000, $y_W^+ = \infty$, T_i = 0.1, $(\rho_W \nu_W)_{SP}$ = 80 g/sm². Enlarged in the wall normal direction by a factor of five.

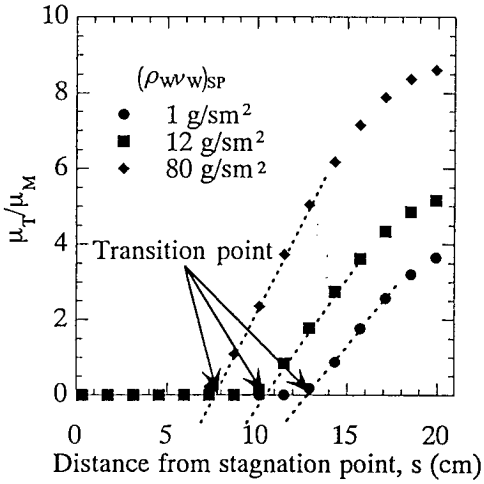

Fig. 6 Eddy viscosity distribution. $Re = 45000$, $y_w^+ = \infty$, $T_i = 0.1$.

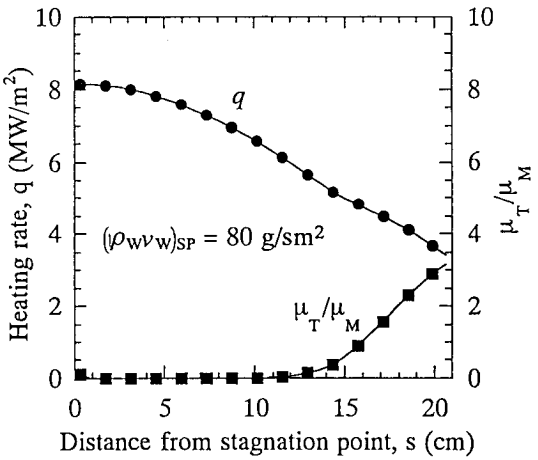

Fig. 7 Distributions of heating rate and eddy viscosity. $Re = 45000$, $y_w^+ = (d/K)(u_\tau/\nu)$, $T_i = 0.1$.

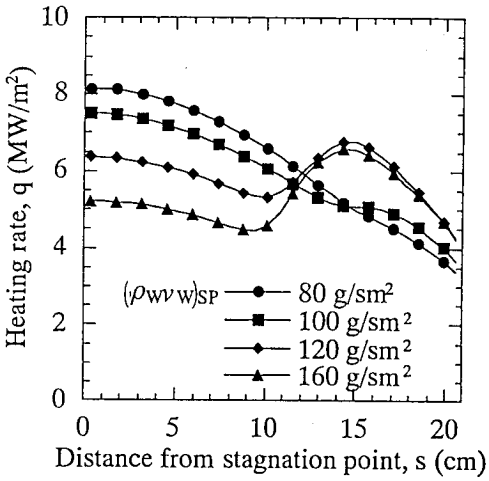

Fig. 8 Heating rate distributions on an ablator surface. $Re = 45000$, $y_w^+ = (d/K)(u_\tau/\nu)$, $T_i = 0.1$.

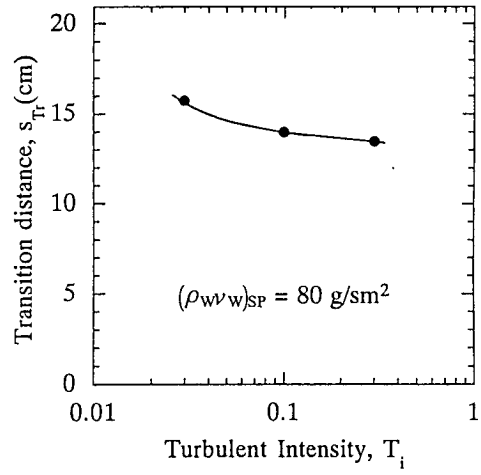

Fig. 9 Surface turbulent intensity and transition distance from stagnation point. $Re = 45000$, $y_w^+ = (d/K)(u_\tau/\nu)$.

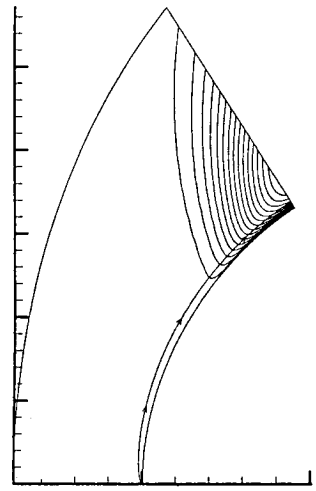

Fig. 10 A streamline of the gas injected near stagnation point and contours of (μ_T/μ_M). $Re = 45000$, $y_w^+ = (d/K)(u_\tau/\nu)$, $T_i = 0.1$, $(\rho_w v_w)_{SP} = 80$ g/sm². Enlarged in the wall normal direction by a factor of 20.

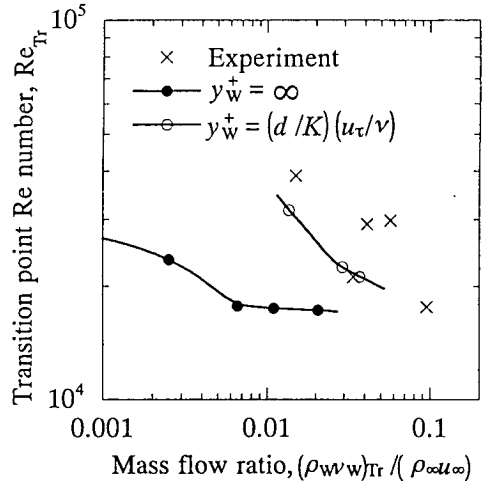

Fig. 11 Transition point Re and injection rate ratio.